OPTICS

Focusing on color: How the eye chooses which wavelength to see best

Benjamin M. Chin[1]*†, Martin S. Banks[1], Derek Nankivil[2], Austin Roorda[1], Emily A. Cooper[1,3]

Humans can see in exquisite detail despite the fact that the eyes' optics can only focus light at a single wavelength at a time. It remains an open question what wavelength is brought into best focus by the human eye. Here, we investigate this question. We used a custom optical apparatus to measure the eye's focusing response (accommodation) to a range of stimuli with different wavelength compositions. We then developed a biologically informed model of the measured responses. Conventional wisdom holds that accommodation works to maximize visual acuity, but our findings suggest otherwise. Rather, our results support alternative lines of evidence that accommodation is guided by chromatic mechanisms that maximize signal quality in a color-opponent channel. Our results challenge prevailing views of oculomotor control and can inform therapeutic interventions for slowing the development and progression of myopia.

INTRODUCTION

To achieve clear vision, the human visual system adjusts the power of the lens within the eye. This process is called accommodation, and it enables the visual system to bring objects at different distances into best focus on the retina (Fig. 1A). The eyes accommodate automatically thousands of times a day (*1*). For example, if a person reads a street sign and then glances at their phone, the eyes adjust focus from far to near in a few hundred milliseconds (*2*, *3*).

Objects in the natural environment, however, can almost never be focused perfectly because visible light consists of many wavelengths. Each wavelength refracts differently through the eye's optics, like the wavelength-dependent refraction through a prism. As a consequence, short wavelengths are brought into focus closer to the lens, and long wavelengths are brought into focus farther from the lens (Fig. 1B). Because the light-sensitive retina is at a fixed distance behind the lens, the retinal images of natural objects often contain substantial amounts of polychromatic blur caused by this so-called longitudinal chromatic aberration (LCA).

Figure 1B illustrates the retinal image of a white letter "E" and the polychromatic blur when the eye brings different wavelengths of the visible spectrum into focus: long wavelengths (red), midrange wavelengths (green/yellow), or short wavelengths (blue). It is not known which response illustrated in the figure best represents the focusing response made by the human visual system, nor what mechanism determines this response.

The prevailing theory has been that the visual system accommodates so as to maximize overall luminance contrast, or image quality, in the retinal image (*4*–*9*). This strategy makes sense because it should maximize visual acuity for the fixated target (*10*, *11*). Luminance, which is the standard measure of visible light intensity, is a weighted sum across visible wavelengths, with middle wavelengths (greenish yellow) receiving the greatest weight (*12*). Consistent with this theory of accommodation, an early study suggested that when people view a stimulus illuminated with white light, the wavelength in best focus falls near the peak of the luminous intensity sensitivity for a range of distances (*13*).

However, recent studies have challenged this theory. Finch *et al.* (*14*), for example, reported that luminous intensity alone is a poor predictor of accommodative responses to stimuli consisting of mixtures of two colors. In addition, several other studies found that polychromatic blur elicited consistent accommodative responses that cannot be explained by luminance-based mechanisms (*15*–*17*). These observations motivate the need to test the luminance-contrast theory and to consider alternative models that are sensitive to the chromatic properties of the stimulus as well.

An understanding of how different wavelengths are focused by the human eye is also relevant for clinical applications that aim to minimize the progression of myopia (nearsightedness). Rates of myopia are increasing rapidly worldwide, suggesting environmental influences (*18*, *19*). This increase is a serious concern because myopic eyes are at greater risk for sight-threatening conditions later in life (*20*). One theory of myopia development states that myopigenic eye growth is triggered when image content is habitually focused behind the retina (*21*–*23*). Recent research suggests, preliminarily, that it may be possible to manipulate this eye-growth signal by altering the wavelength composition of stimuli (*24*–*27*). However, such treatments should be informed by an understanding of which wavelengths are generally focused in everyday environments.

Here, we report oculomotor and perceptual measurements that enabled us to identify the wavelength that the human visual system brings into best focus for a range of stimuli consisting of different light spectra and presented at different distances. We then use these results to understand potential neural mechanisms driving accommodation. Contrary to prevailing theory, the results suggest that accommodative responses are not well explained by a mechanism that maximizes the quality of the luminance information in the retinal image. They are better explained by a mechanism that maximizes a color-opponent signal, supporting converging lines of evidence for a key role of chromatic mechanisms in accommodative control. Last, we modeled and tested the predicted effects of this putative color-opponent mechanism on acuity. We discuss the implications of this mechanism for the role of chromatic information in accommodative control and emerging clinical interventions.

[1]Herbert Wertheim School of Optometry and Vision Science, University of California, Berkeley, Berkeley, CA 94720, USA. [2]Johnson & Johnson Vision Care, Jacksonville, FL 32256, USA. [3]Helen Wills Neuroscience Institute, University of California, Berkeley, Berkeley, CA 94720, USA.
*Corresponding author. Email: bmccis@rit.edu
†Present address: Chester F. Carlson Center for Imaging Science, Rochester Institute of Technology, Rochester, NY 14623, USA.

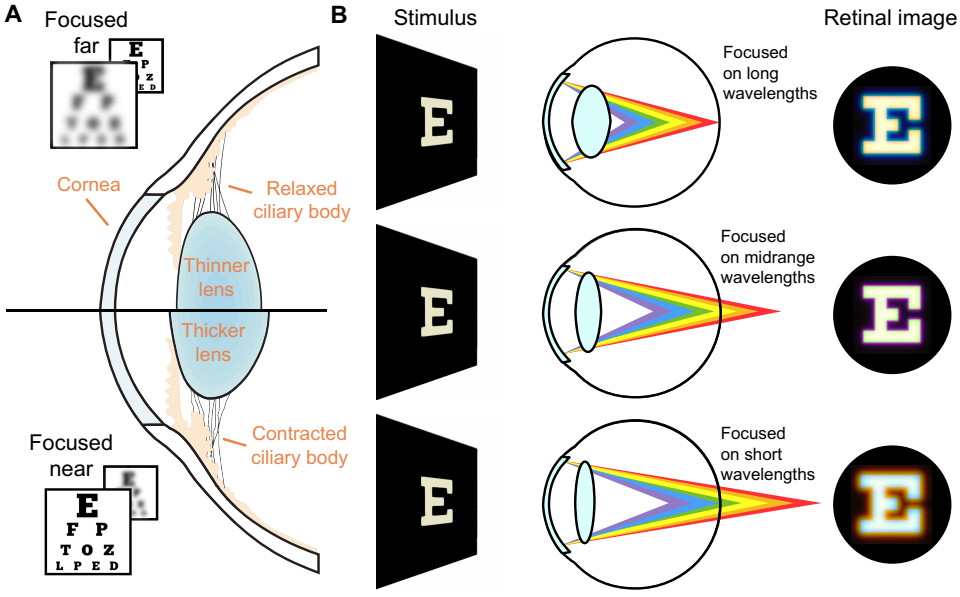

Fig. 1. Accommodation and retinal image focus. (**A**) To focus on objects at different distances, the thickness, and therefore the optical power, of the crystalline lens changes. To focus far, the ciliary body relaxes, the lens thins, and its power decreases. To focus near, the ciliary body contracts, the lens thickens, and its power increases. (**B**) When light from a white E passes through the eye's optics, short wavelengths are brought into focus closer to the lens and long wavelengths farther from the lens. To focus on longer wavelengths, the lens must increase its optical power; to focus on shorter wavelengths, the lens must decrease its power. From top to bottom, we illustrate the retinal images when the eye focuses on long, midrange, or short wavelengths in the visible spectrum, respectively.

RESULTS

Measuring the wavelength in best focus

We used a custom optical apparatus to measure the wavelength in best focus (Fig. 2A). The apparatus allowed us to present stimuli with particular wavelength compositions at different optical distances. Stimuli were presented on a calibrated organic light-emitting diode (OLED) display with narrowband red, green, and blue primaries. A focus-tunable lens enabled precise and rapid control over the optical distance of the stimulus without changing size at the retina.

While the observer focused on the stimulus, a Shack-Hartmann wavefront sensor measured the eye's defocus and other aberrations. The sensor sends a 875-nm collimated beam into the eye and then measures the distortions in the wavefront coming back out. From the wavefront distortions, we compute equivalent defocus and report it in units of diopters (D), which is distance in inverse meters. For example, a defocus measurement of −2 D indicates that the eye's optical power would bring 875-nm light into focus when emitted or reflected by a stimulus 2 D (0.5 m) away.

However, such a measurement indicates defocus only at the nonvisible wavelength of the laser. To determine the visible wavelength that is in best focus for each observer, we also estimated a function describing the relative defocus of the retinal image as a function of wavelength (their LCA curve) (Fig. 2B). This measurement reflects the LCA of the observer's eye and also includes a small amount of LCA inherent to the display system (see Materials and Methods). From any given defocus measurement at 875 nm, this curve allowed us to estimate the amount of defocus at all visible wavelengths on the fovea. We could then solve for the wavelength in best focus at the true stimulus distance. An example is provided in Fig. 2B: 3.5 D is the stimulus distance, and 483 nm is the estimated wavelength in best focus. We repeated the process with colored stimuli at different distances to identify which wavelength was in best focus for each of the stimuli. That is, we determined which scenario from Fig. 1B was most consistent with our observers' accommodative responses.

The wavelength in best focus varies with both stimulus distance and color

We measured the wavelength in best focus in eight observers with normal vision. As illustrated in Fig. 2A, stimuli were three small lowercase letters presented foveally. The stimuli were presented at distances of 29, 40, or 67 cm (i.e., 3.5, 2.5, or 1.5 D). Observers were simply asked to bring the letters into focus. To maximize the effects of chromatic aberration on retinal image quality, we used stimuli with light spectra dominated by long and short visible wavelengths because these have maximal differences in the LCA curve. The stimuli had varying amounts of relative luminance at these wavelengths (red-blue ratio). Half of the stimuli had no additional energy at the peak of the luminous efficiency function (no green), and half had a constant level of energy at this peak (some green). In a series of trials, the stimuli were presented in randomized order with repeated measures for each unique combination of distance and light spectra. We then computed the wavelength in best focus on each trial from the time-averaged defocus measurements as described above. Responses were averaged across repeats for each observer and then averaged across all observers.

There were two clear patterns in the observers' accommodative responses (Fig. 3). First, the average wavelength in best focus across observers tended to be longer for the farthest distance (1.5 D) and shorter for the nearest distance (3.5 D). This is consistent with the so-called "lags and leads" of accommodation, which describe the fact that accommodative gain as a function of distance is often less than one [e.g., (*13*, *28*, *29*)]. These lags and leads are thought to occur because accommodation is biased toward a default distance, or "set point" and deviations from this set point are penalized

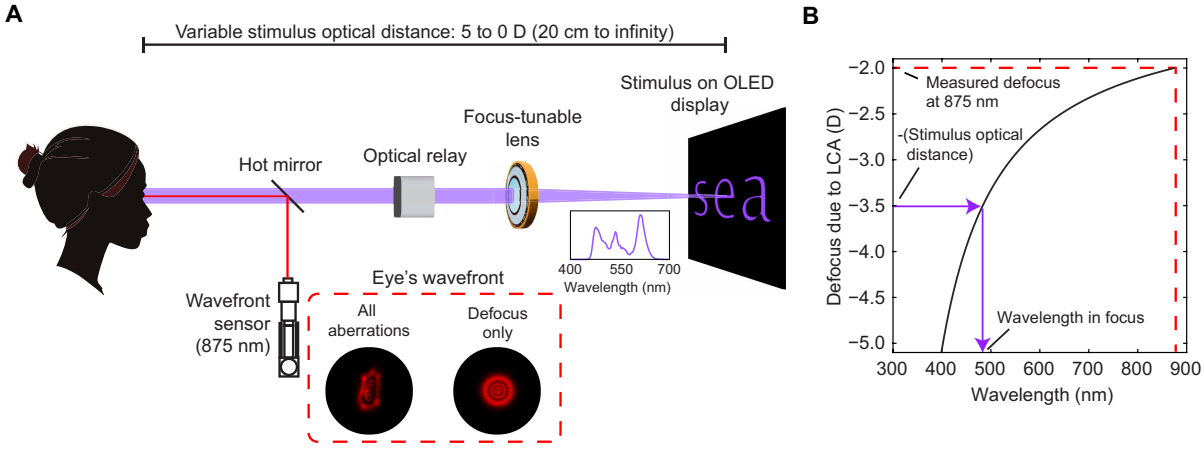

Fig. 2. Experimental apparatus and method for determining wavelength in focus. (**A**) The stimulus was presented on a high-resolution organic light-emitting diode (OLED) display with narrowband primaries modulating the spectral composition in the visible range (purple lines). An optical relay and focus-tunable lens were used to rapidly change the optical distance of the display without changing the size at the retina. Accommodation was measured in infrared (875 nm, red lines) by a Shack-Hartmann wavefront sensor that recorded the full wavefront aberrations of the observer's eye (represented by the point spread function in the left circle), including the defocus aberration (point spread function in the right circle) at this wavelength. (**B**) The LCA curve (black line) specifies the relative defocus between any two wavelengths of light. Given an individual participant's LCA curve, if defocus at one wavelength is known (875 nm, dashed red line), defocus at all other wavelengths can be inferred. The wavelength in focus is the wavelength that is conjugate to the stimulus: For a stimulus located *X* diopters from the eye, the wavelength in focus is the wavelength for which defocus is −*X* D. In this example, *X* is 3.5 D, and the wavelength in best focus is 483 nm.

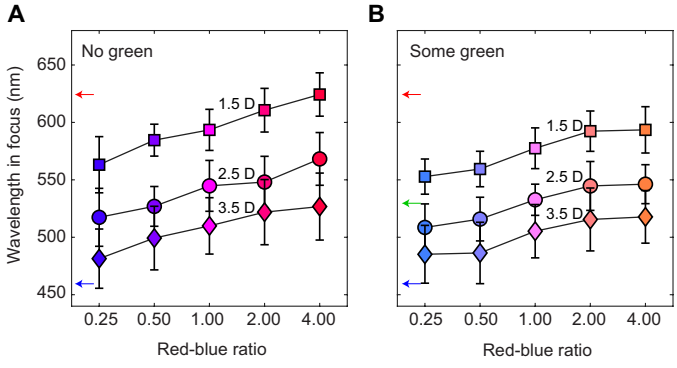

Fig. 3. Estimates of the wavelength in best focus for different stimulus light spectra and distances. Conditions are ordered left to right according to the ratio between the red and blue display primaries. (**A**) Results for stimuli with no energy in the green primary. (**B**) Results for stimuli with the green primary set to a fixed luminance. In both panels, error bars represent 95% confidence intervals, and filled symbols indicate the mean across observers. Arrows indicate peak wavelengths of the red, green, and blue display primaries. Response differences between the three distances reflect the nonunity gain of accommodation as a function of distance. In units of diopters, our participants had a mean gain of 0.74 ± 0.07. Individual values for each participant are shown in table S1.

(*30*, *31*). Overall, the magnitude of the difference between the lag and lead of our closest and farthest stimuli, respectively (typically expressed in diopters), was consistent with expected measurements from prior work [0.53 ± 0.14 D; e.g., (*29*)].

Across all distances, we also consistently observed that the wavelength in best focus changed with the light spectrum: It shifted toward longer wavelengths as the red-blue ratio increased, consistent with previous work (*14*). This pattern occurred whether the green primary was absent (Fig. 3A) or present (Fig. 3B). To test for significance of these effects, we ran a linear mixed effects model with stimulus spectrum (red-blue ratio) and distance as independent variables and with separate intercept terms for each observer. The effect of stimulus color was significant for both stimulus types [no green: $t(4,116) = 3.45$, $P < 0.001$; some green: $t(4,116) = 3.20$, $P = 0.002$]. The effect of optical distance was also significant [no green: $t(2,116) = 10.4$, $P < 0.001$; some green: $t(2,116) = 12.3$, $P < 0.001$]. There were no significant interactions [no green: $t(8,116) = 1.05$, $P = 0.29$); some green: $t(8,116) = 0.61$, $P = 0.54$].

Modeling how wavelength in focus affects the retinal image

We investigated how three potential mechanisms could account for this accommodative behavior. Specifically, we built a bio-optical model for each observer to simulate the effects of wavelength in focus on the retinal image for the stimuli in our experiment (*32*). The model's architecture is shown in Fig. 4A. Bitmaps representing each of the stimuli, along with display calibration measurements, were used to generate radiance maps of the patterned light entering the eye for a set of densely sampled wavelengths. Each observer's LCA and wavefront measurements were used to generate unique point spread functions (PSFs) for each wavelength. The radiance maps were convolved with these PSFs to determine the input to the photoreceptors.

The stimuli were presented in the fovea where there are three photoreceptor types (cones) sensitive to long (L), medium (M), and short (S) ranges of visible wavelengths. Activations of L, M, and S cones are combined into three neural channels, or pathways, that roughly correspond to linear combinations of these activations (*33*). We thus asserted these three possible channels for modeling the signal that drives accommodation, each specified as a different weighted linear combination of the cone mosaics. The L+M channel maps closely to stimulus luminance (*34*). The others are two color-opponent channels: red-green (L−M) and blue-yellow (L+M)−S. Note that our results are the same if the ordering of blue-yellow color opponency is reversed, so we use the (L+M)−S ordering for blue-yellow for ease of comparison with the luminance channel at later stages.

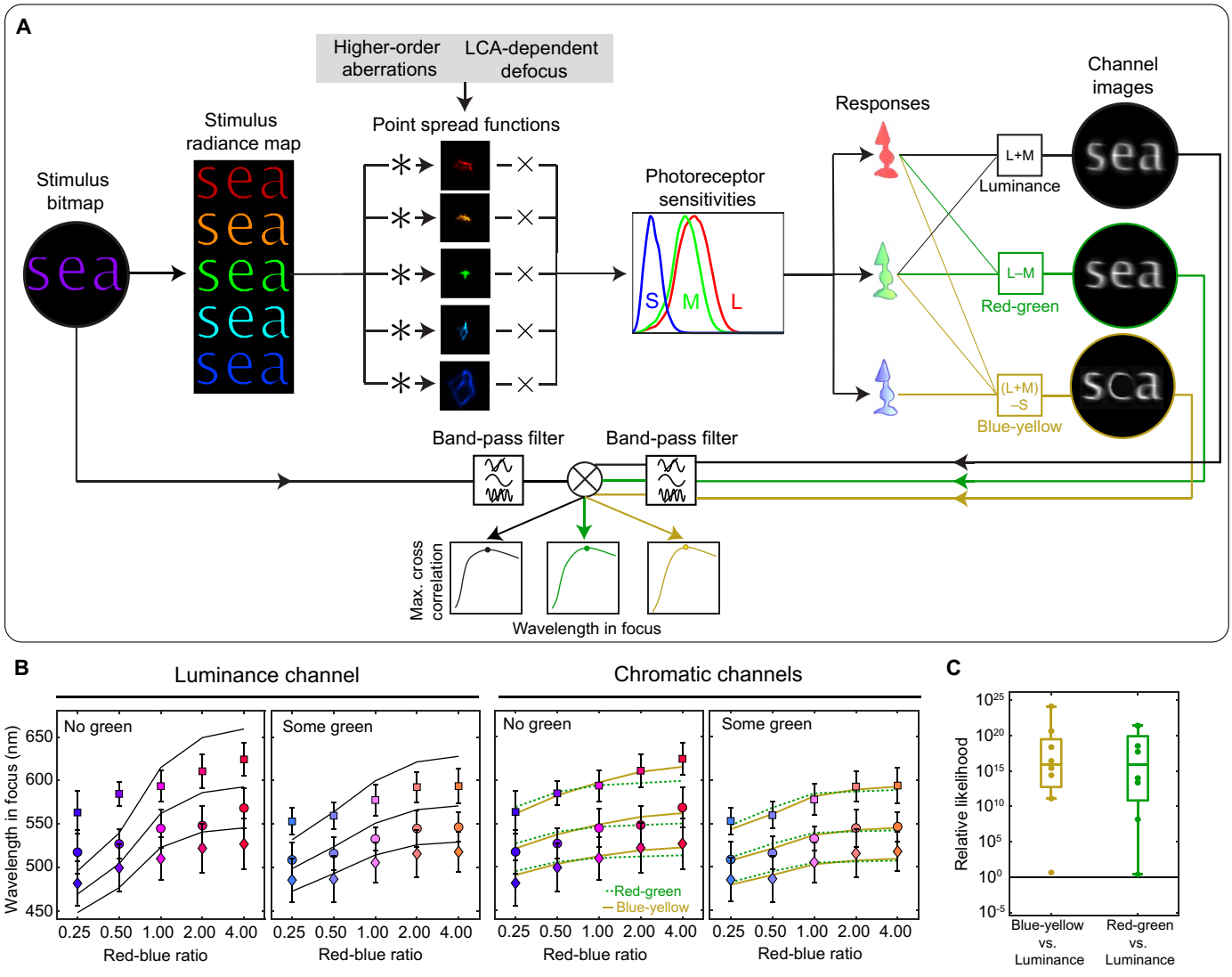

Fig. 4. Schematic of bio-optical model of accommodation and evaluation of fits. (**A**) The stimulus bitmap was converted to a radiance map sampled across visible wavelengths. The result was then convolved with the appropriate point spread function at each wavelength determined by each observer's optical aberrations. The resulting images underwent a weighted sum with weights determined by the spectral sensitivity profiles of each cone photoreceptor type (L, M, and S). The cone responses next underwent an additional weighted sum simulating three neural channels [L+M, L−M, or (L+M)−S]. Last, the channel image as well as the original bitmap were band-pass filtered (to match the spatial frequency sensitivity of accommodation) and cross-correlated with one another. For each channel, the peak value of the aforementioned cross-correlation metric is maximized when a specific wavelength is brought into focus. This constitutes the model prediction, which was determined along with a set of free parameters for each observer. See Materials and Methods for full details. (**B**) The wavelength in best focus, averaged across observers, is plotted as a function of the red-blue ratio. Data points are the observed responses as in Fig. 3. Lines are the averaged model fits. The two left panels show the luminance channel, and the right two show the color-opponent channels (yellow = blue-yellow channel, green = red-green channel). (**C**) Relative likelihood of the best-fitting color-opponent models compared to the best-fitting luminance model. Likelihood values were derived from the difference in Akaike information criterion between the pairs of models. Dots represent values for individual participants and are also shown in table S2.

We created "channel images" simulating the signal in each of these channels for each stimulus. For the S-cone image, we included a central circular region 0.3° in diameter without S-cone activity to represent the S-cone–free zone of the human fovea (*35*, *36*). Signal quality was then quantified by computing the cross-correlation between each channel image and the original stimulus bitmap (*37*–*39*). This approach, like other approaches to quantifying retinal image quality (e.g., Strehl and visual Strehl) takes into account all aberrations of the eye (*40*). However, the cross-correlation approach also takes into account the spatial properties of the stimulus that the other metrics do not. To generate predictions of accommodative response for each stimulus and observer, we iterated over a range of simulated focused wavelengths until we found the one that maximized signal quality. This process was repeated for each of the three neural channels, producing three different model predictions. Each optimization included three to four free parameters capturing individual variation in the relative weighting of the cone classes and distance-dependent biases in accommodation (i.e., lags and leads).

A color-opponent mechanism best explains the responses

The standard theory of accommodation control posits that the visual system accommodates to maximize the quality of the retinal image in terms of luminance (*4*–*9*). Such a mechanism would be optimal for maximizing visual acuity for the stimulus, because visual acuity is primarily determined by luminance contrast (*10*, *11*). The fits for the luminance channel model, averaged across observers, are shown in Fig. 4B (left, black lines) together with the average responses. The best-focused wavelength for this model varied more with red-blue ratio than the measured responses. Specifically, the model predicted that the peak wavelength of the red primary would be brought into focus when the red primary had higher luminous intensity and that the peak wavelength of the blue primary would be in focus when the blue primary had higher luminous intensity (assuming no lags and leads). In other words, the luminance model predicts a larger effect of red-blue ratio on accommodation than we observed. This finding is consistent with the results reported by Finch *et al.* (*14*).

Inspired by previous work showing chromatic effects on accommodation, we next investigated the predictions of color-opponent mechanisms. The results are shown in the right panels of Fig. 4B (yellow lines and green lines). Both color-opponent models provided a better fit to the data because they make smaller changes in response to changes in red-blue ratio than the luminance model did. Hence, both models outperformed the luminance-based model for all observers (Fig. 4C). For six observers, the blue-yellow mechanism was the best fit, and for two, the red-green mechanism was best.

These results suggest that accommodation does not necessarily maximize the quality of the luminance information in the retinal image. Instead, our data are more consistent with maximizing signal quality based on color-opponency. In the next section, we examine the ability of the color-opponent channel model to account for performance on a visual acuity task.

Model evaluation on independent measurements of acuity

A luminance-based mechanism for driving accommodation should maximize visual acuity because acuity is primarily determined by luminance contrast (*10*, *11*). Thus, our modeling results raise the possibility that accommodation might not always maximize visual acuity for the fixated stimulus. To investigate this, we had the same group of observers perform an acuity test and examined how well their performance maximized acuity.

In this task, we presented a fixation target at a fixed optical distance (40 cm, 2.5 D). The red-blue ratio was always one-to-one. After observers indicated that they had focused the target, it was removed and a square wave grating was presented very briefly. The grating had the same red-blue ratio as the fixation target but could appear at different distances from the target (*28*) (Fig. 5A). The grating was flashed too briefly for it to trigger an accommodative response. Observers indicated whether the grating was clockwise or counterclockwise from vertical. Performance was indexed by proportion correct in the orientation-discrimination task. If observers accommodated to maximize visual acuity for stimuli at the distance of the fixation target, then the best performance in the orientation task should occur when the grating and fixation target are at the same distance. Because the stimuli consisted of two primaries with quite different wavelengths, one might expect to observe two distances at which acuity was higher than at other distances: one peak

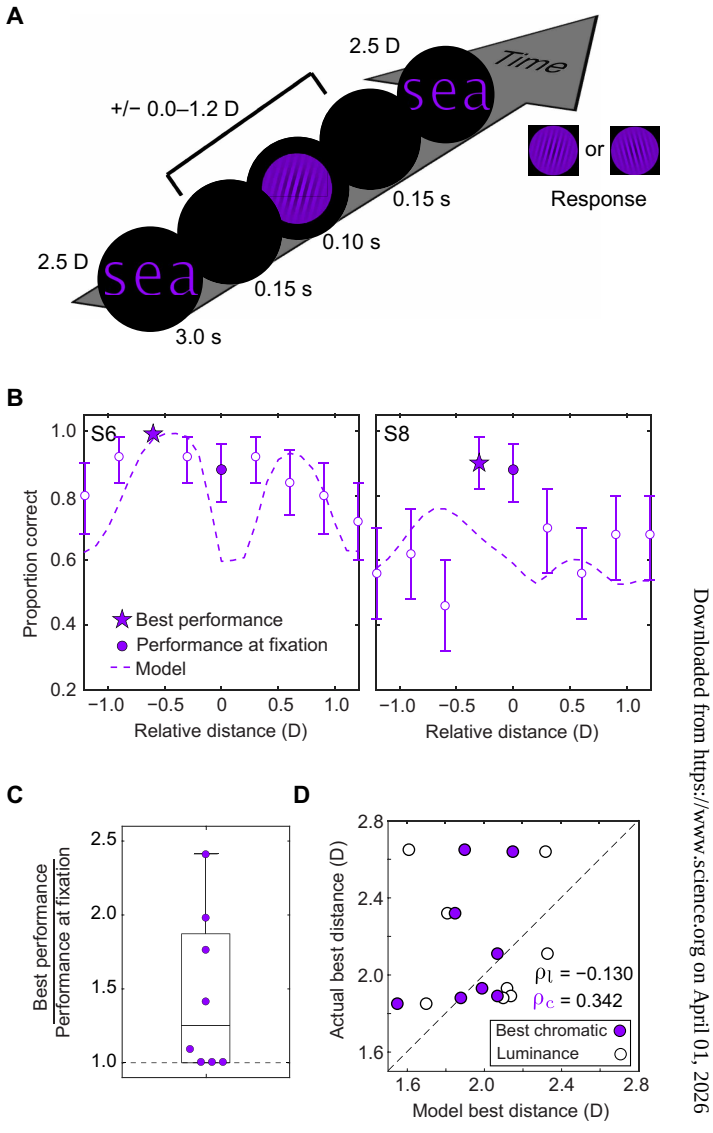

Fig. 5. Visual performance and accommodative responses. (**A**) Observers focused on a three-letter stimulus. Then, the screen was blanked briefly, and a square wave grating was flashed at various distances relative to the three letters. Observers indicated on each trial whether the grating was clockwise or counterclockwise from vertical. (**B**) Data from two example observers. The data points are proportion correct in the orientation-discrimination task, plotted as a function of the relative distance between the fixation stimulus (always at 2.5 D) and the grating. Negative and positive values correspond respectively to grating distances farther and closer than the fixation stimulus, respectively. Error bars are 95% confidence intervals as determined by the binomial distribution. Dashed lines represent predictions of the data by the best-fitting color-opponent model for that observer. (**C**) Best performance relative to performance at distance of fixation stimulus for each observer. The ordinate values are maximum performance (d-prime) divided by performance (again d-prime) when the fixation stimulus and flashed grating were at the same distance. These values are associated with the filled star and filled circle markers in (B), respectively. Individual values are shown in table S3. (**D**) Predicted versus actual distances at which best performance occurred for best-fitting color-opponent model for each observer from the previous experiment (filled) and the luminance model (unfilled). Correlations between the predicted and observed best distances are shown for the luminance (ρ_l) and best chromatic (ρ_c) models.

corresponding to having the red primary in focus and another to having the blue primary in focus.

There were notable individual differences in the distance at which best performance occurred. These differences likely derive from differences in both monochromatic and chromatic aberrations, since both types of aberration can affect acuity and are known to vary across individuals. Example performance is shown in Fig. 5B for two observers with qualitatively different patterns (circular markers). One observer appeared to maximize performance when the grating probe and the accommodative stimuli were at approximately the same distance (S8), while the other observer appeared to maximize their performance when the grating was closer than the fixation target (S6). Overall, four observers achieved best performance and thus maximized acuity at the fixation stimulus distance, while the other four observers did so at a different distance (Fig. 5C, ratio of the filled circles and stars in Fig. 5B). To assess the robustness of these results, we bootstrapped each participant's response data (see Materials and Methods for details) and determined the probability that acuity was maximized at the fixation distance. For the four participants with ratios near 1 in Fig. 5C, this probability was high (37 to 100%), while for the other four participants, this probability was low (0.2 to 10%).

We next examined whether the individual differences that we observed in the acuity experiment could be explained by performance in the first (accommodation) experiment. To do so, we built an ideal observer model of the acuity task. For each real observer, we first generated the predicted retinal images cast by the acuity probe (the grating) in the two orientations. These images were created from the individually measured aberrations and fitted accommodative response to a red-blue ratio stimulus of 1 at 2.5 D derived from the first experiment. To make an ideal observer prediction, we then computed the predicted d-prime for these retinal image pairs on the basis of a template matching model with a single overall efficiency parameter (*41*, *42*). Separate predictions were made for the best color-opponent model per observer in the first experiment and for the luminance model (dashed lines in Fig. 5B represent the color model). In Fig. 5D, the model predictions for the distance at which best performance should occur are plotted against the true best distances for all observers for the color-opponent model (filled circles) and for the luminance model (unfilled circles). For the color-opponent model, the root mean square (RMS) error between the predictions and the acuity data was 0.38 D, and the correlation (ρ_c) between them was 0.34 ($P = 0.41$). These values indicated a qualitatively smaller prediction error than the luminance model [RMS error: 0.46 D, $t(7) = 1.30$, $P = 0.24$], which also had a lower correlation with the data ($\rho_l = -0.13$, $P = 0.76$). Preliminarily, these models appear to align with some observers' performance better than others, which may reflect inaccuracies in the predicted retinal image, variation in people's accommodative behavior across tasks, or other higher-level differences in task performance. Hence, this final analysis provides initial evidence—but not yet conclusive evidence—that acuity as well as accommodative responses may be explained by a color-opponent neural channel.

DISCUSSION

The clarity of human vision is limited by the eye's chromatic aberrations. These aberrations shape the quality of the retinal image, introducing blur at nonfocused wavelengths. Despite the loss of image quality from this polychromatic blur, the target of focus tends to appear subjectively sharp, highlighting the differences between the retinal images and the ultimate percept (*43*–*46*). For example, selectively blurring chromatic information in natural scenes has unexpectedly little effect on perceived sharpness (*47*–*49*). At the same time, there is compelling evidence that the visual system uses this polychromatic blur to support visual function (*15*–*17*). In this study, we find evidence for a color-opponent mechanism that uses this blur to determine which wavelength is brought into best focus.

The influence of a color-opponent mechanism on the wavelength in best focus is plausible given existing evidence that the visual system uses polychromatic blur in retinal images—that is, the colorful fringes seen in the images in Fig. 1B—as a directional cue for driving dynamics in accommodation. In particular, accommodative responses to stimuli that are moving in depth are impaired when these color fringes are eliminated (*50*, *51*) and aided when they are simulated (*15*, *16*). Theories of how the visual system uses these color fringes typically invoke the notion of a comparison between contrast at short wavelengths and long wavelengths (*16*, *52*). Color opponency mechanisms, known to underlie two of the three cardinal visual channels, are a natural fit for such a purpose (*33*). In essence, we propose that the accommodative response maximizes a signal indicating the amount of chromatic contrast created by LCA.

Signals from both blue-yellow and red-green opponent mechanisms explained our data well, and we do not heavily favor one color-opponent model over the other on the basis of our data. Specifically, six observers were better fit with a blue-yellow model, and the other two were better fit with a red-green model. We do, however, speculate that S cones provide a particularly useful signal because the effect of chromatic aberration is greatest at short wavelengths. Although S-cone responses appear too sluggish to support rapid accommodative responses, they are known to contribute during accommodation to static stimuli (*53*) such as those used in our experiments. Involvement of S cones is also consistent with empirical findings that accommodative sensitivity peaks for relatively low spatial frequencies (*54*, *55*). The spatial frequencies at which peak accommodative sensitivity occurs (3 to 4 cycles/deg) are in between the peak of the contrast sensitivity function for S cones [<1 cycle/deg; (*56*, *57*)] and the peak of the luminance contrast sensitivity function (3 to 6 cycles/deg). Thus, the involvement of an S-cone signal provides an appealing potential explanation for why accommodative responses are biased toward lower spatial frequencies: Perhaps accommodative contrast sensitivity reflects a compromise between the sensitivity of two poles of a blue-yellow channel.

In Fig. 6, we aim to illustrate an intuition for the effects of this putative mechanism on accommodative behavior and defocus. In brief, because of differences in the retinal images between S cones and L/M cones, the blue-yellow color-opponent model penalizes accommodative behavior that brings shorter wavelengths into focus. For an example observer, Fig. 6A shows the signal quality as a function of simulated wavelength in focus for three stimulus red-blue ratios, based on the luminance model (top) and blue-yellow opponency model (bottom). While the wavelengths associated with best quality are similar for redder stimuli (red-blue ratio = four-to-one and one-to-one), the blue-yellow opponency mechanism predicts longer wavelengths in focus when the stimulus is quite blue (red-blue ratio = one-to-four). Figure 6B shows the retinal signal quality for a single "a" in our stimulus with a high red-blue ratio of four-to-one, as estimated for luminance alone (L+M), S cones alone (−S), and blue-yellow

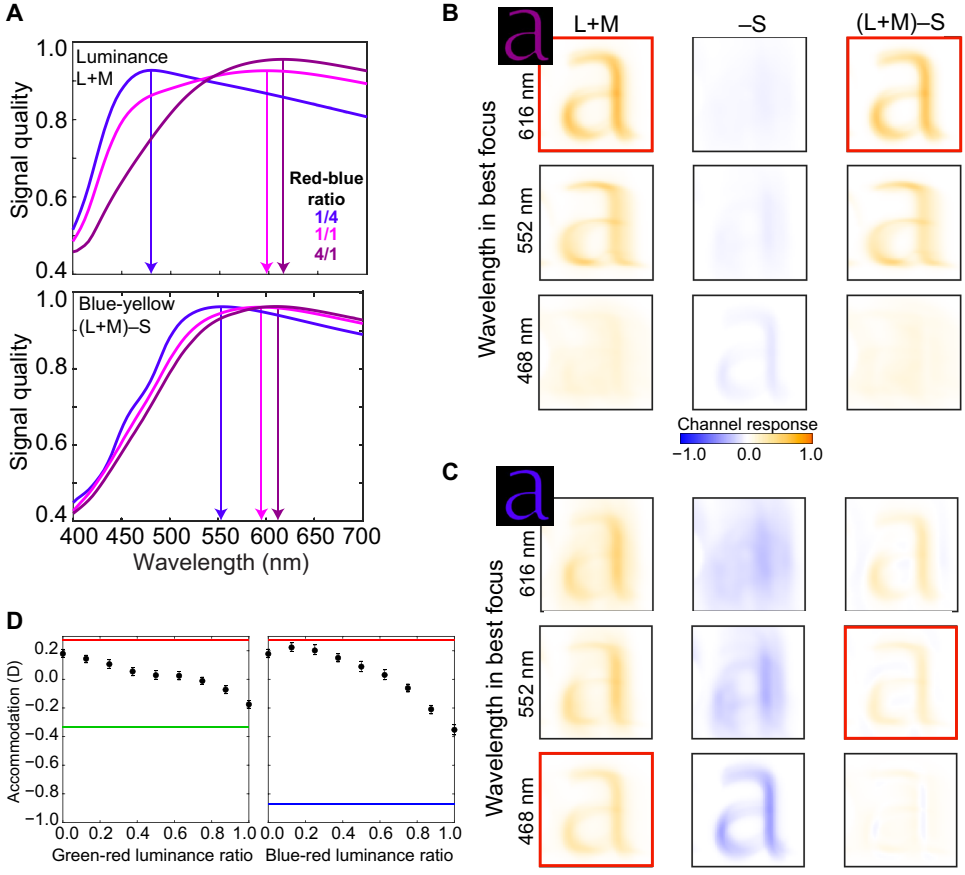

Fig. 6. Outputs of the luminance and blue-yellow color-opponent mechanisms for an example observer. (**A**) Signal quality in the luminance channel (top) and blue-yellow opponent channel (bottom) as a function of wavelength is shown for three stimuli varying in their red-blue ratio. Arrows indicate the predicted wavelength in focus for each stimulus. (**B**) For a stimulus with a high red-blue ratio, we show color maps of channel response for an L+M channel, an S-only channel (mapped to negative values), and an (L+M)−S channel. Focusing a long wavelength of 616 nm maximizes signal quality in both the L+M and (L+M)−S channels (red boxes). (**C**) For a stimulus with a low red-blue ratio, focusing a short wavelength of 468 nm (bottom row) maximizes signal quality in the L+M channel, but signal quality in the combined (L+M)−S channel will be poor. Best signal quality in the (L+M)−S channel is instead obtained when a middle wavelength of 552 nm is in focus. (**D**) A subset of the data from Finch *et al.* (*14*) are replotted, showing relative accommodation for different ratios of red versus green LEDs (left) and red versus blue LEDs (right). Solid lines indicate accommodation required to focus the peak wavelength of each primary assuming the average human LCA function. Their data indicate a bias away from blue, consistent with a blue-yellow opponent mechanism.

opponency [plotted as (L+M)−S]. The quality of the "a" is visually best for both luminance and blue-yellow mechanisms when ~616 nm is in focus. However, the results diverge for a bluish "a" (red-blue ratio of one-to-four; Fig. 6C). For the luminance model, the bluish letter is best quality when the dominant wavelength is in focus (~468 nm). However, for the blue-yellow opponency model, this strategy will simultaneously maximize signal quality of the S-cone output and L+M output, therefore reducing signal quality when the difference (L+M)−S is computed. Hence, for the blue-yellow opponency model, a better compromise can be obtained when middle wavelengths are placed into focus; this yields a relatively sharp L+M image while maintaining a blurry opponent S-cone image. The blue-yellow mechanism avoids focusing on blue light as compared to the luminance mechanism.

Note that the effect of accommodative lags and leads will be to shift the selected wavelength in focus toward a shorter or longer wavelength along the curves in Fig. 6A. The fact that these curves tend to be shallow near their peaks suggests that modest lags and leads, like those observed in our study, may not markedly reduce signal quality. The existence and cause of lags and leads remain a topic of debate (*28*), but regardless, they indicate that the wavelength in best focus is dependent on both the stimulus light spectrum and the stimulus distance. Despite these differences, the relative effects of light spectrum in our data were remarkably similar at each stimulus distance, suggesting that these effects are consistent across a range of experiences. Lags and leads can also be described in terms of a single accommodative gain: a multiplicative scaling factor that relates the actual accommodative response to the accommodative demand of the stimulus. We wondered whether applying a realistic accommodative gain factor might meaningfully improve the fit of the luminance model, which otherwise predicts a larger overall range of responses than we observed empirically (Fig. 4B). Since accommodative demand is defined by the amount of defocus aberration required to form a sharp image, the same gain factor should apply whether the change in demand arises from stimulus distance or from the spectral composition of the stimulus. However, when we

applied our empirically measured gain (0.74 ± 0.07) to the luminance model predictions, the predicted response range (0.74 + 0.20) remained much larger than that observed in our data (0.32 ± 0.12). We conclude that conventional lags and leads are not large enough to bring the luminance model into alignment with the responses observed to changes in stimulus color.

Our results and model also provide an alternative interpretation of recent work from Finch *et al.* (*14*), which examined accommodative responses to mixed pairs of narrowband light-emitting diodes (LEDs). Finch *et al.* (*14*) also found that accommodative power varies smoothly with the proportion of long/short wavelengths but did not report the wavelength in best focus. They provisionally explained their data with a model that maximizes luminance image contrast at a single low spatial frequency (2 or 4 cycles/deg). However, that model predicted larger variation in responses than were observed in the data. To ensure that we were not overlooking alternative plausible models, we nonetheless reran our simulations incorporating their proposed band-pass luminance model. The resulting mean likelihood ratios with models based on both color-opponent channels still robustly favored a color-opponent model (fig. S1). The observed pattern of responses in the data of Finch *et al.* (*14*) contains a signature of a blue-yellow signal–based model: Shorter wavelengths tend not to be brought into focus (see Fig. 6D for an example of their data with this property). Thus, we conclude that the color-opponency model potentially provides a more economical account for accommodative responses in both studies.

Our signal quality metric (the maximum normalized cross-correlation between the encoded image and the stimulus image) was chosen to ensure that the model reflects the spatial structure of the stimulus. This approach effectively performs a form of template matching, with the original stimulus image serving as the template. While it is uncertain whether the visual system has direct access to such a template, this seems plausible for familiar stimuli like letters. That is, the observer might infer the sharp-edged font of the true stimulus. Moreover, template-matching models have been shown to capture human performance in other visual tasks, including target detection and discrimination (*38*, *41*, *42*). Our main conclusions remain unchanged when using an alternative image-quality metric that does not take the stimulus spatial properties into account (the Strehl ratio; see fig. S2). We also note that metrics like Strehl or visual Strehl assume that the visual system has access to the eye's PSF—an assumption that is itself not guaranteed. Thus, determining which internal representation best reflects the input used by the visual system for optimizing focus, and other visual tasks, remains an open question. However, the conclusions of the current analysis do not depend on the specific assumptions made about this representation.

There are several important caveats and open questions raised by this work. First, we measured accommodation under monocular viewing. Under natural binocular viewing, accommodative responses are neurally coupled to binocular eye movements (vergences), which may alter the wavelength in focus. Second, our stimuli necessarily relied on the three narrowband peaks of our display primaries rather than the broadband spectra reflected by natural surfaces (*58*). Although confirming generalization to arbitrary spectra will require future work, the broadband nature of natural light has an important implication for retinal image quality. When natural surfaces reflect substantial energy near the middle visible wavelengths, accommodating between red and blue (as observed for many of our stimuli) will tend to yield relatively good retinal image quality. Thus, even if luminance image quality is not explicitly optimized when determining the wavelength in focus, it may frequently be preserved during natural vision. Third, our stimuli were all small, foveally presented, and contained a single light spectrum. During natural vision, the visual system will receive stimuli across the visual field with spatial variation in color and will need to integrate this information across space to determine the best accommodative response. For example, it is known that stimulation of peripheral vision can drive accommodation in addition to the foveal stimulation used in our study (*59*–*61*). Relatively less, however, is known about accommodative responses to mixtures of colors and different spatial patterns, which warrants future investigation. Even if the wavelength in best focus does change with these additional viewing parameters, understanding the mechanism governing the influence of chromatic contrast on its own can help us work toward a multimodal model of all the cues that lead to accommodative responses.

Last, we want to highlight the potential translational relevance of these results for emerging eye care research. The incidence of myopia is increasing rapidly, which suggests that environmental changes in our society are an important cause (*18*, *19*). Both wavelength-dependent blur and "near work"—which refers to focusing on content in the peripersonal space, as during reading or hand-held device use—are thought to exacerbate the risk for developing myopia (*24*, *62*–*69*). In our study, the stimulus associated with the shortest wavelength in focus was the nearest, bluest stimulus (Fig. 3). This is important because when shorter wavelengths are in focus on the retina, this generates hyperopic defocus that is hypothesized to trigger the eye growth that leads to myopia (*21*–*23*). Recently proposed myopia mitigation strategies that use chromatic filtering may therefore function by shifting the wavelength in focus back toward longer wavelengths, particularly during near work (*24*–*27*). Our data and modeling can help us understand quantitatively how different ways of filtering chromatic content affect retinal defocus by enabling researchers and engineers to estimate the wavelength in focus for a given stimulus, rather than assuming it is always the same middle wavelength. It is also possible that the accommodative behavior determining wavelength in best focus differs between myopes and nonmyopes (our sample was not sufficient to test this and contained no high myopes) Together, these observations highlight the need to consider the full spectral distribution of lighting encountered in the everyday environment to understand potential effects of the environment on eye growth.

MATERIALS AND METHODS

Observers

Eight adults (seven females, one male) between 18 and 30 years of age (mean: 24.75 ± 3.73 years) participated. All had normal or corrected-to-normal visual acuity and normal color vision. Observers requiring correction were all moderate myopes and wore contact lenses. Because the study entailed a demanding set of measurements and tasks, we used an extensive screening process. An additional nine individuals were recruited but did not pass this screening (described in more detail below). Three observers who passed the screening were excluded because of data quality issues: Two had large errors in their measured accommodation (up to ±2D from the stimulus), and one had behavioral data that could not be reliably fitted for threshold estimation. Thus, in total 20 individuals were recruited,

11 completed the study, and 8 were included in the final dataset. All study procedures were approved by the Institutional Review Board at the University of California, Berkeley (Institutional Review Board Protocol ID: 2023-03-16136), and all research participants gave informed consent.

Stimulus presentation and accommodation measurements

Stimuli were displayed using a custom apparatus (Fig. 2A) described in detail by Roorda *et al.* (*70*). The apparatus has an active-matrix OLED display panel with three narrowband primaries (peaks: red = 624 nm; green = 530 nm; blue = 460 nm; full width at half maximum: red = 43 nm; green = 24 nm; blue = 24 nm). Observers viewed this display through an optical relay system with an exit pupil diameter of 4 mm that resulted in a circular field of view with a 3° diameter and a pixel size of 0.23 arc min. The maximum luminance of the primaries viewed through the system was as follows: red = 1.4 cd/m^2, green = 4.1 cd/m^2, and blue = 0.4 cd/m^2. The optical distance of the stimulus was adjusted with a focus-tunable lens (Model EL-10-30, Optotune, Dietikon, Switzerland) placed conjugate to the observer's eye, allowing rapid changes between optical infinity and 20 cm (0 to 5 D) without changes in visual size at a response time of ~15 ms. We computed the system LCA using Zemax optical design software. The Zemax model of the system included the details of the Optotune lens, which were provided by the manufacturer. The estimated system LCA between the peaks of the red and blue display primaries was 0.3 D. Accommodative responses were measured by a Shack-Hartmann wavefront sensor incorporated into the optical path via a hot mirror, which recorded the eye's wavefront aberrations at 875 nm at 30 Hz, sampled via a lenslet array with an effective separation of 200 μm (linear sampling density of five measurements per millimeter). Each observer was fitted with a custom bite bar, which they used to precisely maintain eye position relative to the apparatus. All stimuli were presented, and measurements were taken with the right eye while the left eye was covered.

Measurement 1: Defocus at 875 nm for polychromatic stimuli at different distances

Trial structure

In a series of repeated trials, we measured the eye's wavefront as observers viewed colored letters presented at different optical distances. Each trial had the following structure (Fig. 7A): Observers were instructed to focus on a three-letter stimulus spanning 1° wide end-to-end (stroke width ~2 arc min) against a black background. They were given as much time as necessary to bring the stimulus into focus. They were instructed to press a button once the stimulus was in focus and to keep it in focus for the next 3 s. The button press initiated a recording from the wavefront sensor for the 3-s period. Then, the stimulus disappeared for half a second before the next trial began.

Stimuli

The spectral composition of the stimulus was varied from trial to trial by manipulating the relative intensities of the three primaries, resulting in 12 possible combinations (Table 1). On a given trial, all letters had the same spectrum. These spectra contained different red-blue luminance ratios. For five of them, the red-blue ratio varied from 0.25 to 4.0 in five equal log-spaced steps while the green primary was set to zero (no green). To assess whether accommodative responses changed in the presence of middle wavelengths, we also included these same five red-blue ratios while setting the green primary to constant luminance (some green). We did not include conditions that were purely red or purely blue because our pilot testing found that in our system many naive observers could not accommodate accurately to narrowband stimuli with single peaks (*51*, *71*). This limitation has been reported in previous work [but see (*72*) for a recent counterexample using an open-field stimulus presentation]. We also included two control stimuli: a stimulus with a flat spectrum across all primaries to assess wavelength in focus for comparison with previous work and a stimulus with a red-blue ratio of 1 and no green but with lower luminance to examine the effects of luminance on accommodation.

Each of these 12 spectra was presented at three different optical distances: 67 cm (1.5 D), 40 cm (2.5 D), and 29 cm (3.5 D), yielding 36 conditions. There were six repeats per condition, for a total of 216 trials. In each of the condition repeats, the stimulus pattern was one of six possible permutations of the lowercase letters "s," "e," or "a." These letters were selected because they contain a range of line orientations and lack ascenders or descenders. Trials were run in a randomized block order, with each block consisting of nine trials of the same color with three repeats of each optical distance. Figure 7B shows some example measurements.

The optical properties of our apparatus and the intensity of the blue primary limited the luminances at the observer's eye. Thus, to achieve the desired red-blue ratios, all of our stimuli had total luminances that were 1.2 cd/m^2 or less. These low values would be a concern if accommodative performance was hampered by low luminance. However, accommodative performance is relatively invariant with changes in luminous intensity when luminance is ~0.5 cd/m^2 or greater (*73*). To check, we ran a control analysis, comparing measured defocus for a red-blue ratio of 1 at luminances of 0.8 and 0.5 cd/m^2; performance was not notably different between these two conditions [$t(7) = 1.23$, $P = 0.26$, higher luminance mean defocus = 2.44 ± 0.12 D, lower luminance mean defocus = 2.47 ± 0.14 D]. Furthermore, our stimuli should occupy the rod-free zone of the retina because of their small size and foveal presentation, eliminating the possibility that sensitivity in any condition is driven by mesopic or scotopic sensitivity.

Performance screening

Before beginning the experiment, observers practiced bringing stimuli into focus in the experimental apparatus. They viewed a natural image that oscillated sinusoidally between 0 and 3.5 D and were asked to keep it in focus. Next, the screening task consisted of a series of trials in which the observer viewed the three-letter stimulus with each display primary at 0.40 cd/m^2. The stimulus was randomly presented at 1.5, 2.5, or 3.5 D. After 3 s, the screen was blanked for 100 ms, and a Landoldt "c" 5.75 arc min in width (between the 20/20 and 20/25 rows on a Snellen chart) was flashed for 100 ms in one of four orientations. The task was to report the orientation. Because accommodation happens on a timescale much slower than 100 ms, and the stimulus contained energy across a range of visible wavelengths, the observer could only reliably answer correctly if they had accurately accommodated near the stimulus distance. Participants passed the screening if they made three or fewer errors over 30 trials. Five recruited individuals were excluded on this basis.

Wavefront analysis

We fit the measured wavefronts at each time point as a weighted sum of the first 65 Zernike polynomials, the standard orthogonal basis set (*74*). Specifically, an automated script was used to analyze the infrared camera images and extract the displacements of the wavefront sensor illuminant through the lenslets. We then found the

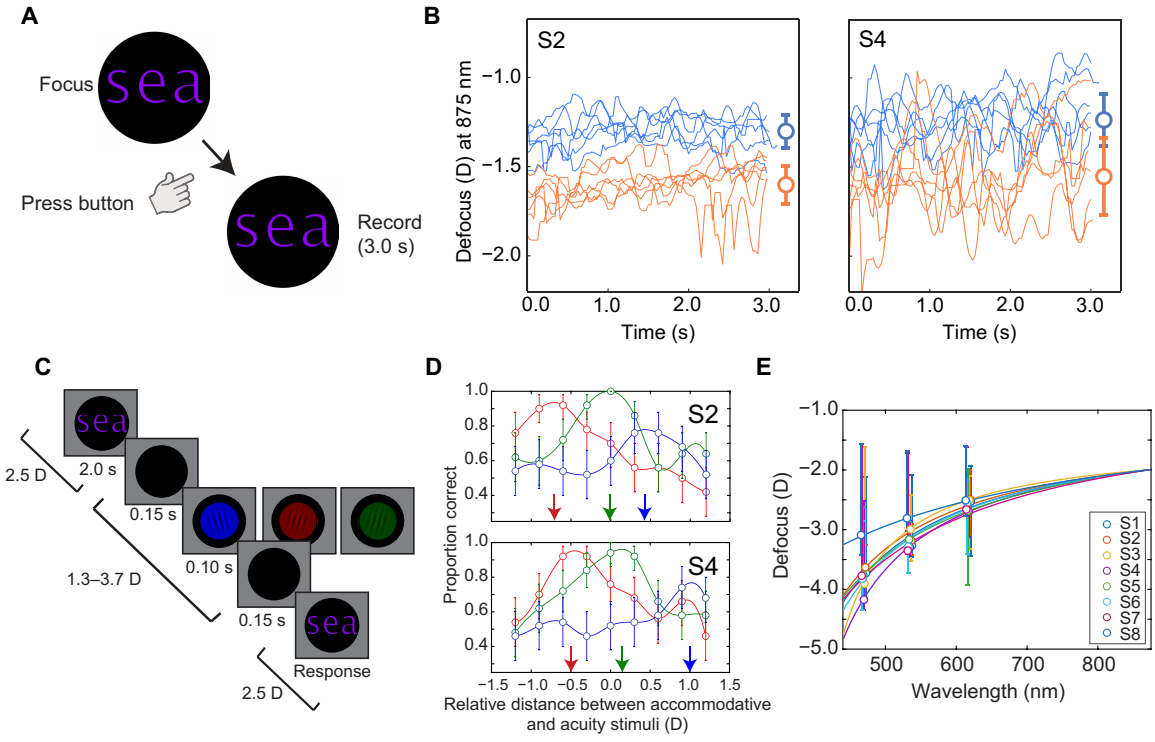

Fig. 7. Methods and example raw data for the measurements of defocus and LCA. (**A**) In the task for measuring defocus, observers accommodated to a three-letter stimulus and pressed a button to initiate the wavefront recording when the stimulus appeared in focus. Stimulus spectra are listed in Table 1. (**B**) Examples of continuous traces of the eye's defocus recorded by the wavefront sensor at 875 nm for two stimulus conditions and two observers. Circular markers on the right represent means of the traces, and error bars represent SDs. (**C**) In the task used to measure LCA, observers viewed a three-letter stimulus at 2.5 D for 2 s before it briefly disappeared and a square wave grating was flashed. The observer indicated the orientation of the grating. The distance and color of the grating varied from trial to trial. (**D**) Example performance data from the same two observers shown in (B). Each line shows the proportion correct for the red, green, or blue primary for each relative distance of the grating. Arrows indicate the estimated distance at which best performance was reached for each color. (**E**) LCA functions for all eight observers based on performance in the task in (C). Each data point corresponds to the negative of a best-performance distance [arrows in (D)]. For visualization, all functions have been shifted so their value at 875 nm is 2 D. In (D) and (E), error bars represent 95% confidence intervals.

Table 1. Luminances and red-blue ratios in the experiment. Each row indicates a stimulus condition, and columns show the luminance of the red, green, and blue primaries in candelas per square meter, the red-blue ratio, and the total luminance.

	Red luminance (cd/m^2)	Green luminance (cd/m^2)	Blue luminance (cd/m^2)	Red-blue ratio	Total luminance (cd/m^2)
No green	0.10	0.00	0.40	0.25	0.5
	0.20	0.00	0.40	0.50	0.6
	0.40	0.00	0.40	1.00	0.8
	0.40	0.00	0.20	2.00	0.6
	0.40	0.00	0.10	4.00	0.5
Some green	0.10	0.20	0.40	0.25	0.7
	0.20	0.20	0.40	0.50	0.8
	0.40	0.20	0.40	1.00	1.0
	0.40	0.20	0.20	2.00	0.8
	0.40	0.20	0.10	4.00	0.7
Control: Flat spectrum	0.40	0.40	0.40	1.00	1.2
Control: Luminance	0.25	0.00	0.25	1.00	0.5

wavefront function most consistent with these displacements. Coefficients for each of the 65 Zernike polynomials were optimized by minimizing the RMS error.

The coefficient on the fifth Zernike polynomial indicates the defocus aberration at 875 nm, while the other coefficients capture the higher-order aberrations of the eye, such as astigmatism and spherical aberrations. For each observer in each trial, we averaged the fitted fifth coefficient over all valid time points (Z_5) and obtained the average measured equivalent defocus at 875 nm in diopters ($\widehat{d}_{875}$) using the following standard conversion

$$\widehat{d}_{875} = 4\sqrt{3}\left(\frac{2}{u}\right)^2 Z_5 \quad (1)$$

where u corresponds to the pupil diameter in millimeters. Although the participants' pupils were always larger than 4 mm, we analyzed and computed the defocus over a fixed 4-mm subpupil since that corresponded to the diameter of the collimated light entering the observer's eye from our apparatus. The full fitted wavefront over the 4-mm subpupil was used later in the retinal image modeling (see below).

We excluded data points on which the analysis software identified blinks or was unable to fit a wavefront to the image captured by the sensor. We also excluded trials in which the magnitude of estimated measured defocus at 550 nm was more than ±2 D from the true stimulus distance. For these large deviations, all wavelengths within the visible spectrum (400 to 700 nm) are out of focus, suggesting an erroneous measurement or that the observer did not succeed in bringing the stimulus into focus. These exclusions consisted of 10 of 1584 trials.

Measurement 2: Longitudinal chromatic aberrations

Task

Once average defocus at 875 nm was measured for each stimulus, we needed to characterize the LCA curve to solve for the visible wavelength in best focus (Fig. 2B). While average LCA curves are available in the literature (*75*), we decided that we should measure individual LCA curves because prior studies show substantial individual variability [see the supplement of (*76*) for a summary of nine prior studies that measured LCA]. In a separate session, we estimated the relative defocus as a function of wavelength for each observer. We used a modified version of a task developed by Labhishetty *et al.* (*28*), which leverages the effects of defocus on acuity to measure points along each observer's LCA curve (Fig. 7C). In practice, this measurement is very similar to those used for the final acuity task reported in the results (diagrammed in Fig. 5A). On each trial, observers began by fixating and accommodating to a three-letter stimulus of the same size and pattern used in measurement 1. We used the balanced red-blue ratio stimulus with no green for consistency with measurement 3 (described below). This stimulus was always presented at an optical distance of 40 cm (2.5 D). After 2 s, the screen was blanked for 150 ms, during which the optical distance was changed randomly by 0, ±0.3, ±0.6, ±0.9, or ± 1.2 D. Then, a 15-cycle/deg square wave grating was presented for 100 ms, followed by another 150-ms blank period before the word stimulus reappeared. The color of the grating was generated with a single primary: red, green, or blue. It was placed on a luminance pedestal of 0.20 cd/m^2 and a diameter of 1°. The grating orientation was 15° to the left or right of vertical. The observer reported the grating orientation, and each condition was repeated 50 times in a random order. Feedback was given after each trial. The brief presentation time of the grating ensured that observers did not change their accommodation to focus on it. Because of higher-order aberrations, the distance of best acuity can depend on the spatial frequencies and orientations contained within the stimulus. Thus, we aimed to match these properties as closely as possible between the accommodative stimulus (three letters) and the probe (grating). Specifically, the half width of 1 cycle in the 15-cycle/deg square wave grating was approximately equal to the stroke of each letter in the three-letter stimulus. The critical part of the square wave stimulus is the difference between its two potential orientations. The letter stimuli had a large amplitude at 15 cycle/deg because of their stroke width. Thus, the difference spectrum in the grating test stimulus had the greatest amplitude at 15 cycle/deg where there was substantial energy in the spectrum of the letters.

Contrast calibration

Before starting the main measurements, we determined the grating contrast for each observer yielding 85% performance when each primary was in sharp focus. The calibration task was identical to the main task except the accommodative stimulus and the grating were always matched in color (red-red, green-green, and blue-blue), and the contrast of the grating was manipulated rather than the relative distance. Six contrast levels spanning 20 to 100% contrast were used, with 20 trials per contrast level. To estimate thresholds, a Weibull function was fit to the data using log-likelihood as the objective function. Four observers who had passed the screening for measurement 1 were unable to reach 85% performance level for at least one of the three colors and were thus excluded from measurement 2. For the included observers, mean Michelson contrast thresholds for each color were 0.66 ± 0.14 for red, 0.63 ± 0.11 for green, and 0.70 ± 0.14 for blue.

Analysis

For each observer and each primary peak wavelength (λ_p), we fit spline functions (using not-a-knot end conditions via MATLAB's interp1 function) to the proportion of the time they responded correctly as a function of the grating optical distance (Fig. 7D). For each primary peak wavelength, we defined the measured defocus ($\widehat{d}_p$) as the negative of the optical distance in diopters associated with the highest proportion correct on the spline. These three data points $\left(\lambda_p, \widehat{d}_p\right)$ were then used to constrain a fitted LCA curve. LCA curves were parameterized with a standard three-parameter equation that maps out the relationship between wavelength in nanometers (λ) and predicted defocus in diopters due to LCA $\left[d(\lambda)\right]$ (*75*)

$$d(\lambda) = c - \frac{a}{\lambda - b} \quad (2)$$

where a, b, and c are free parameters. Here, a and b describe the nonlinear mapping between wavelength and defocus, while c shifts the overall amount of defocus, depending on the accommodative state of the eye. Note that these LCA measurements necessarily will include the LCA inherent to the optical system (0.3 D between the peak wavelengths of the red and blue display primaries). We use the full behaviorally measured LCA so as to incorporate both the effects of the system and the eye's optics, as is appropriate for accurately modeling the retinal image. The data and resulting fits for each observer are plotted in Fig. 7E. For visualization, we have aligned each observer's data by setting c such that there is 2 D of defocus at 875 nm to match Fig. 2B. While some individual measurements had relatively

high uncertainty (error bars), the average magnitude and variability of our LCA measurements are similar to values reported by others (*70*, *77*–*81*).

Determining wavelength in best focus

As described in Results, for each observer and each stimulus condition, after we determined the average measured defocus at 875 nm ($\widehat{d}_{875}$), we then determined the unique value of c (c') such that the fitted LCA curve passed through the point (875, $\widehat{d}_{875}$)

$$c' = \widehat{d}_{875} + \frac{a}{875 - b} \tag{3}$$

This allowed us to rewrite Eq. 2 to solve for the estimated wavelength in best focus $\widehat{\lambda}_{\text{best}}$, that is, the wavelength with a defocus value corresponding to the stimulus distance (d_{stim}) when the LCA curve passes through the measured defocus at 875 nm

$$\widehat{\lambda}_{\text{best}} = \frac{a}{c' - d_{\text{stim}}} + b \tag{4}$$

As a reminder, we included stimuli with equal luminance in each primary as a control condition. Consistent with early studies of accommodation (*13*), when observers accommodated to these stimuli, on average, the wavelength in best focus was 570.9 ± 14.0 nm for stimuli at 1.5 D, 527.8 ± 18.2 nm for stimuli at 2.5 D, and 499.0 ± 24.5 nm for stimuli at 3.5 D.

To test for significant differences between the wavelength in best focus as a function of red-blue ratio, we ran a generalized linear mixed model with wavelength in focus as the dependent variable. Optical distance, red-blue ratio, and their interaction were the regressors. A separate intercept was modeled for each observer. For the "no green" conditions, coefficient estimates were as follows: 40.60 ± 3.91 for optical distance, 17.19 ± 4.98 for red-blue ratio, and 2.00 ± 1.90 for their interaction. The estimate of the fixed-effects intercept was 630.64 ± 13.07 and the SD associated with the random effects was 22.77. For the "some green" conditions, coefficient estimates were as follows: 35.24 ± 2.85 for optical distance, 11.65 ± 3.64 for red-blue ratio, and 0.85 ± 1.38 for their interaction. The estimate of the fixed-effects intercept was 608.91 ± 11.30 and the SD associated with the random effects was 23.89. Tests of significance are reported in Results.

Retinal image modeling

Retinal image modeling was done with the aid of the ISETBIO toolbox (see Fig. 4A) (*32*). First, we computed a discretely sampled radiance map of the on-display stimulus $\left[I_{\text{stim}}(x, y, \lambda)\right]$, where x and y denote spatial locations in arc minutes sampled in steps of 0.23 arc min (angles subtended by each display pixel when viewed in our apparatus) and λ is sampled in steps of 4 nm from 380 to 780 nm. For each observer and stimulus, we then simulated the radiance pattern falling on the retina $\left[I_{\text{r}}(x, y, \lambda)\right]$ via two-dimensional (2D) convolution of the stimulus radiance map at each wavelength with the full PSF $\left[\text{PSF}(x, y, \lambda)\right]$ of the eye at that wavelength

$$I_{\text{r}}(\boldsymbol{x}, \boldsymbol{y}, \lambda) = \left[I_{\text{stim}}(\boldsymbol{x}, \boldsymbol{y}, \lambda) *_{2\text{D}} \text{PSF}(\boldsymbol{x}, \boldsymbol{y}, \lambda)\right] t(\lambda) \text{ for all } \lambda \tag{5}$$

Here, $I_{\text{r}}(\boldsymbol{x}, \boldsymbol{y}, \lambda)$ denotes the full map at a single wavelength, and $t(\lambda)$ reflects the lens transmittance at that wavelength—this transmittance is lowest at short visible wavelengths and increases for longer wavelengths. The symbol $*_{2\text{D}}$ represents two-dimensional convolution in the horizontal and vertical spatial (but not wavelength) dimensions x and y. The PSF was computed from the wavefront aberration measurements described above using the Fourier method (*82*) assuming uniform spatial transmittance across the pupil, which was a 4-mm-diameter circle.

To model the effects of different wavelengths in focus (λ_{focus}) on the retinal images, for each observer, a range of PSFs associated with different λ_{focus} values were created (as shown in Fig. 4A). To create these PSFs, we assume that higher-order aberrations, which were measured at 875 nm, are the same at all visible wavelengths (*83*). For each λ_{focus}, we determined the relative defocus for all other wavelengths due to LCA by applying Eq. 2 as follows

$$d_{\text{relative}}(\lambda, \lambda_{\text{focus}}) = d(\lambda) - d(\lambda_{\text{focus}}) \tag{6}$$

and converted to the Zernike coefficient by inverting Eq. 1. By definition, relative defocus is 0 when $\lambda = \lambda_{\text{focus}}$. To model the coefficients on all nondefocus polynomials for each observer, we averaged the fitted coefficients across all valid time points in all trials. Note that this approach assumes that the defocus term is the only term that changes with accommodation, which is not strictly the case (*29*, *84*–*86*). However, we chose to average the higher-order coefficients rather than model their relationship with accommodation so as to avoid overparameterizing our model, and because defocus is by far the primary coefficient affected by accommodation. We then used the full set of coefficients to compute the associated PSFs for each wavelength as described above and performed the convolution yielding the retinal radiance map $I_{\text{r}}(x, y, \lambda)$.

Each retinal radiance map was then converted into three "cone images" $\left[L(x, y), M(x, y), \text{and } S(x, y)\right]$ incorporating the spectral sensitivity of the three classes of photoreceptor cones in the human eye. These sensitivities also include all other spectral modulations except the lens transmittance that was modeled separately as described above. Each cone image represents the stimulus as it is encoded by each of the cone types

$$L(x, y) = \int_{\lambda=0}^{\infty} I_{\text{r}}(x, y, \lambda) l(\lambda) d\lambda \tag{7}$$

$$M(x, y) = \int_{\lambda=0}^{\infty} I_{\text{r}}(x, y, \lambda) m(\lambda) d\lambda \tag{8}$$

$$S(x, y) = \int_{\lambda=0}^{\infty} I_{\text{r}}(x, y, \lambda) s(\lambda) d\lambda \tag{9}$$

Here, $l(\lambda)$, $m(\lambda)$, and $s(\lambda)$ are the spectral sensitivity functions of the L, M, and S cones, respectively. While we do not explicitly model the different sampling densities of the cone types, when we modeled signals used for accommodation (described below), we applied a low-pass filter that truncated the spatial frequencies to a range below the acuity thresholds for L and M cones and close to the S cone threshold (*87*). For the S-cone image, we modeled a blank central circular region 0.3° in diameter to simulate the S-cone–free zone found in the human fovea.

These cone images were then combined into channel images $I_{\text{c}}(x, y)$. A channel image was a weighted sum of the three cone images

$$I_c(x,y) = w_L L(x,y) + w_M M(x,y) + w_S S(x,y) \quad (10)$$

where the weights w_L, w_M, and w_S are free parameters. When modeling the luminance channel mechanism (L+M), the weights w_L and w_M are both constrained to be positive, with w_S set to 0. Since the relative contributions of the L- and M-cone pathways to luminance vary across individuals (*34*, *88*), we had one free parameter per observer that was the ratio between weights on the L and M cones. When modeling the blue-yellow opponent channel [which we formulated as (L+M)−S], the weights w_L and w_M were both constrained to be positive, while w_S was constrained to be negative. The blue-yellow channel image had a blank central region corresponding to the S-cone–free zone. For the red-green opponent channel (L−M), w_L was constrained to be positive, w_M was constrained to be negative, and w_S was 0.

Our model assumes that the visual system aims to maximize signal quality in one of these channel images. We defined signal quality for a given wavelength in focus $\left[\text{Quality}(\lambda_{focus})\right]$ as the peak normalized absolute cross-correlation between a channel image and a bitmap indicating the original stimulus pattern in normalized units (I_{map}) (*37*–*39*). Before computing this cross-correlation, we limited both the channel image and the bitmap to the range of spatial frequencies known to drive accommodation

$$\text{Quality}(\lambda_{focus}) = \max\left[\left|\left(I_c * h\right) \star \left(I_{map} * h\right)\right|\right] \quad (11)$$

Here, h is a band-pass spatial filter capturing the observation that accommodation is primarily driven by medium spatial frequencies (*54*, *55*). The asterisk indicates convolution, and the star indicates normalized cross-correlation. We used the MATLAB normxcorr2 function, which normalizes the resulting value such that the autocorrelations at zero lag equal one. The band-pass filter was determined by fitting the data published by Owens (*55*). In the Fourier domain, the modulation transfer function (MTF) of the filter defined over spatial frequencies f_x and f_y was

$$\text{MTF}_h(f_x,f_y) = \exp\left\{-\frac{1}{2}\left[\frac{\log\left(\sqrt{f_x^2+f_y^2}\right) - \log(\mu)}{\sigma}\right]^2\right\} \quad (12)$$

where $\mu = 2.42$ and $\sigma = 1.11$. This function has a full width at half maximum of ~8 cycle/deg.

In practice, by maximizing the absolute value of the cross-correlation, we ensure that our model was agnostic to the ON/OFF structure of the channel [i.e., (L+M)−S and S−(L+M) were treated equivalently]. In the (L+M)−S–based model, the central 0.3° of the original stimulus pattern I_{map} was also blank to match the simulated S-cone–free zone.

On a given trial, the predicted wavelength in best focus λ_{best} is the wavelength λ_{focus} that maximizes signal quality of the channel image

$$\lambda_{best} = \underset{\lambda_{focus}}{\text{argmax}}\ \text{Quality}(\lambda_{focus}) \quad (13)$$

From the predicted wavelength in best focus λ_{best}, the predicted defocus measured by the wavefront sensor at 875 nm (d_{875}) was calculated as

$$d_{875} = d_{relative}(875, \lambda_{best}) - \left[d_{stim} - k(d_{stim})\right] \quad (14)$$

Here, the first term reflects the relative defocus between λ_{best} and 875 nm according to the observer's LCA curve. Subtracting d_{stim} anchors this relative defocus to the actual stimulus distance in diopters. We also include $k(d_{stim})$ as a bias term that accounts for lags and leads in accommodation: the observation that people tend to accommodate less to nearby stimuli and more to farther-away stimuli (*13*, *28*, *29*). Together, these elements act as the c parameter in Eq. 2. The bias term was modeled as a linear function of stimulus distance, which was forced to be the same for all stimulus spectra at a given distance

$$k(d_{stim}) = m d_{stim} + g \quad (15)$$

Model fitting

To fit the model, for each channel (luminance, blue-yellow, and red-green), we optimized the cone weighting parameters w_L, w_M, and w_S and the lag/lead parameters m and g to minimize the RMS error between the predicted defocus at 875 nm (d_{875}) and average measured defocus ($\hat{d}_{875}$) across all stimuli. In practice, we were able to reduce the number of free parameters because the model's predictions only change with the relative ratios of the three cone weighting parameters, not their overall magnitude. That is, for a given ratio of the three cone weights, applying a scale factor to all three weights will not change the model predictions. Thus, the luminance and red-green model had only one free cone weighting parameter each, and the blue-yellow model had two. All three models share a common free parameter, the L/M weight ratio (0.75 ± 0.14 for the luminance model, 0.74 ± 0.05 for the red-green model, and 0.71 ± 0.14 for the blue-yellow model). The blue-yellow model has an additional free cone weighting parameter, the S/(L+M) weight ratio (−0.88 ± 0.25).

Whereas the best-fitting cone weighting parameters were optimized using a grid search, the two free parameters for lags and leads were optimized using MATLAB's fmincon function for every iteration of the grid search. This implementation amounted to a compromise between comprehensiveness and computational efficiency. For two observers, S3 and S8, the grid search was performed twice because the initial bounds on the S/(L+M) weight parameter were too constrained to fit their data. Estimated parameters for lags and leads followed expected patterns from prior work showing a small lag at 555 nm that grew with stimulus distance. Lags were small for the blue-yellow opponency–based model (mean = −0.04 ± 0.07 D for 67 cm, mean = −0.31 ± 0.10 D for 40 cm, and mean = −0.57 ± 0.16 D for 29 cm), for the red-green opponency–based model (mean = −0.14 ± 0.05 D for 67 cm, −0.40 ± 0.10 D for 40 cm, and mean = −0.66 ± 0.16 D for 29 cm), and for the luminance-based model (mean = 0.11 ± 0.13 D for 67 cm, −0.15 ± 0.13 D for 40 cm, and mean = −0.41 ± 0.16 D for 29 cm). Although prior work suggests that these effects may be much smaller during natural vision, our stimulus was viewed monocularly at relatively low luminance, which may be a condition more likely to reveal lags and leads (*73*, *89*).

Model comparison

The Akaike information criterion (AIC) of each model was calculated as

$$\text{AIC} = 2v - 2\ln\left(\hat{L}\right) \quad (16)$$

where v is the number of free parameters and $\hat{L}$ is the maximized value of the likelihood function for the model. The relative likelihood between the models was computed as

$$\hat{L}_a / \hat{L}_b = \exp\left(\frac{\mathrm{AIC}_b - \mathrm{AIC}_a}{2}\right) \quad (17)$$

where $\hat{L}_a$ was either the red-green or blue-yellow model and $\hat{L}_b$ was the luminance model.

Measurement 3: Acuity as a function of stimulus distance

The acuity measurement task was designed to test the prediction that participants did not always accommodate to maximize acuity. This measurement (illustrated in Fig. 5A), was identical to the LCA measurement task except both the grating and accommodative word stimuli were purple (0.40 cd/m^2 for both the red and blue primaries). As described above, we aimed to match the spatial frequencies and orientations in the two stimuli as closely as possible. Contrast levels for the acuity stimuli were again set according to 85% thresholds measured using the same calibration task described above. We defined the distance of best acuity as the optical distance at which observers responded with the highest proportion correct.

To test whether best performance was different from performance at the distance of the accommodative word stimulus, we computed the ratio between each observer's best sensitivity and their sensitivity at the stimulus distance. We defined sensitivity as d-prime and converted each observer's empirical proportion of correct responses to d-prime values $\hat{Q}$ as follows

$$\hat{Q} = 2\Phi^{-1}(n) \quad (18)$$

where n is the proportion of correct responses and Φ^{-1} is the inverse cumulative normal distribution.

We then conducted a bootstrap analysis to assess the robustness of any deviations from a ratio of 1. For each participant, trials across all distance conditions were resampled with replacement 1000 times. For each resampling, proportion correct was recalculated at each distance. Then, we calculated the percentage of samples in which the highest proportion correct was achieved when the grating was at the same distance as the accommodative stimulus.

Ideal observer model of acuity task

We modeled the discriminability between any two images $\left[I_1(x,y)\right.$ and $\left.I_2(x,y)\right]$ for an ideal observer under the assumption of independent Poisson noise at each pixel (*41*, *42*). According to this model, the observer's sensitivity is determined by sum of d-prime values across all paired pixel locations in the images

$$Q = \int_{x=0}^{\infty}\int_{y=0}^{\infty} q(x,y)\,dxdy \quad (19)$$

Here, Q denotes the global d-prime of the ideal observer and $q(x,y)$ denotes the pixel-wise d-primes. These pixel-wise values are determined by the differences between the two images and are scaled by an efficiency parameter σ_a

$$q(x,y) = \frac{\left[I_2(x,y) - I_1(x,y)\right]\ln\left[I_2(x,y)/I_1(x,y)\right]}{\sigma_a\left\{\left[I_2(x,y) + I_1(x,y)\right]\ln^2\left[I_2(x,y)/I_1(x,y)\right]\right\}^{1/2}} \quad (20)$$

To create an ideal observer prediction for each real observer in our study, individualized retinal radiance maps were computed for the square wave grating at both orientations (cl = clockwise rotation, cc = counterclockwise rotation). These radiance maps were converted to luminance images by applying the $V(\lambda)$ function using the same approach used to apply the individual cone sensitivity functions $\left(I_1 = I_{\mathrm{cl}}, I_2 = I_{\mathrm{cc}}\right)$. The predicted d-prime was computed as described above.

To obtain the appropriate PSFs for generating these images, we assumed that during this task, the defocus at 875 nm was equal to the defocus determined from the fits of the best-fitting chromatic and luminance models to the observer's data from the first experiment $\left(d_{875}\right)$. The defocus at each other wavelength and stimulus distance was therefore computed as

$$d\left(\lambda, d_{\mathrm{stim}}\right) = d_{\mathrm{relative}}(\lambda, 875) + \left[d_{875} + d_{\mathrm{stim}}\right] \quad (21)$$

The first quantity captures the relative defocus between every wavelength and the wavelength at which defocus was measured, and the second bracketed quantity asserts the defocus state of the eye relative to the stimulus. Last, we fit the model to the data by optimizing the free parameter σ_a to minimize the RMS error between measured and modeled d-prime values.

Supplementary Materials

This PDF file includes:

Tables S1 to S3
Figs. S1 and S2

REFERENCES

1. W. W. Sprague, E. A. Cooper, S. Reissier, B. Yellapragada, M. S. Banks, The natural statistics of blur. *J. Vis.* **16**, 23 (2016).
2. F. W. Campbell, G. Westheimer, Dynamics of accommodation responses of the human eye. *J. Physiol.* **151**, 285–295 (1960).
3. S. Phillips, D. Shirachi, L. Stark, Analysis of accommodative response times using histogram information. *Am. J. Optom. Arch. Am. Acad. Optom.* **49**, 389–400 (1972).
4. W. R. Bobier, M. C. Campbell, M. Hinch, The influence of chromatic aberration on the static accommodative response. *Vision Res.* **32**, 823–832 (1992).
5. W. N. Charman, J. Tucker, Accommodation and color. *J. Opt. Soc. Am.* **68**, 459 (1978).
6. F. J. Rucker, The role of luminance and chromatic cues in emmetropisation. *Ophthalmic Physiol. Opt.* **33**, 196–214 (2013).
7. L. Stark, Y. Takahashi, Absence of an odd-error signal mechanism in human accommodation. *I.E.E.E. Trans. Biomed. Eng.* **12**, 138–146 (1965).
8. A. Troelstra, B. L. Zuber, D. Miller, L. Stark, Accommodative tracking: A trial-and-error function. *Vision Res.* **4**, 585–594 (1964).
9. J. M. Wolfe, D. A. Owens, Is accommodation colorblind? Focusing chromatic contours. *Perception* **10**, 53–62 (1981).
10. M. J. Morgan, T. S. Aiba, Positional acuity with chromatic stimuli. *Vision Res.* **25**, 689–695 (1985).
11. K. T. Mullen, The contrast sensitivity of human colour vision to red-green and blue-yellow chromatic gratings. *J. Physiol.* **359**, 381–400 (1985).
12. *Proceedings of the 8th Session*, Cambridge, England, September 1931 (Commission Internationale de l'Eclairage, 1931).
13. A. Ivanoff, Focusing wave-length for white light. *J. Opt. Soc. Am.* **39**, 718 (1949).
14. A. P. Finch, M. Fernandez-Alonso, A. K. Kirby, J. C. A. Read, G. D. Love, Focusing on mixed narrow band stimuli: Implications for mechanisms of accommodation and displays. *J. Vis.* **24**, 14 (2024).
15. S. A. Cholewiak, G. D. Love, P. P. Srinivasan, R. Ng, M. S. Banks, Chromablur: Rendering chromatic eye aberration improves accommodation and realism. *ACM Trans. Graph.* **36**, 1–12 (2017).
16. S. A. Cholewiak, G. D. Love, M. S. Banks, Creating correct blur and its effect on accommodation. *J. Vis.* **18**, 1 (2018).
17. P. B. Kruger, S. Mathews, K. R. Aggarwala, D. Yager, E. S. Kruger, Accommodation responds to changing contrast of long, middle and short spectral-waveband components of the retinal image. *Vision Res.* **35**, 2415–2429 (1995).
18. Committee on Focus on Myopia: Pathogenesis and Rising Incidence, Board on Behavioral, Cognitive, and Sensory Sciences, Division of Behavioral and Social Sciences and Education, National Academies of Sciences, Engineering, and Medicine, *Myopia: Causes, Prevention, and Treatment of an Increasingly Common Disease* (National Academies Press, 2024); https://nap.nationalacademies.org/catalog/27734.

19. B. A. Holden, T. R. Fricke, D. A. Wilson, M. Jong, K. S. Naidoo, P. Sankaridurg, T. Y. Wong, T. J. Naduvilath, S. Resnikoff, Global prevalence of myopia and high myopia and temporal trends from 2000 through 2050. *Ophthalmology* **123**, 1036–1042 (2016).
20. A. E. G. Haarman, C. A. Enthoven, J. W. L. Tideman, M. S. Tedja, V. J. M. Verhoeven, C. C. W. Klaver, The complications of myopia: A review and meta-analysis. *Invest. Ophthalmol. Vis. Sci.* **61**, 49 (2020).
21. F. Schaeffel, A. Glasser, H. C. Howland, Accommodation, refractive error and eye growth in chickens. *Vision Res.* **28**, 639–657 (1988).
22. D. Troilo, J. Wallman, The regulation of eye growth and refractive state: An experimental study of emmetropization. *Vision Res.* **31**, 1237–1250 (1991).
23. C. F. Wildsoet, Neural pathways subserving negative lens-induced emmetropization in chicks—Insights from selective lesions of the optic nerve and ciliary nerve. *Curr. Eye Res.* **27**, 371–385 (2003).
24. T. J. Gawne, Z. She, T. T. Norton, Chromatically simulated myopic blur counteracts a myopiagenic environment. *Exp. Eye Res.* **222**, 109187 (2022).
25. S. Ravikumar, E. N. Harb, K. E. Molina, S. E. Singh, J. Segre, C. F. Wildsoet, Ocular biometric responses to simulated polychromatic defocus. *J. Vis.* **24**, 3 (2024).
26. Z. She, T. J. Gawne, The parameters governing the anti-myopia efficacy of chromatically simulated myopic defocus in tree shrews. *Transl. Vis. Sci. Technol.* **13**, 6 (2024).
27. B. Swiatczak, F. Schaeffel, Myopia: Why the retina stops inhibiting eye growth. *Sci. Rep.* **12**, 21704 (2022).
28. V. Labhishetty, S. A. Cholewiak, A. Roorda, M. S. Banks, Lags and leads of accommodation in humans: Fact or fiction? *J. Vis.* **21**, 21 (2021).
29. S. Plainis, H. S. Ginis, A. Pallikaris, The effect of ocular aberrations on steady-state errors of accommodative response. *J. Vis.* **5**, 7 (2005).
30. F. M. Toates, A model of accommodation. *Vision Res.* **10**, 1069–1076 (1970).
31. F. M. Toates, Accommodation function of the human eye. *Physiol. Rev.* **52**, 828–863 (1972).
32. N. P. Cottaris, H. Jiang, X. Ding, B. A. Wandell, D. H. Brainard, A computational-observer model of spatial contrast sensitivity: Effects of wave-front-based optics, cone-mosaic structure, and inference engine. *J. Vis.* **19**, 8 (2019).
33. A. Stockman, D. H. Brainard, "Color vision mechanisms" in *OSA Handbook of Optics: Vision and Vision Optics Vol. III*, M. Bass, Ed. (McGraw-Hill, 2010), pp. 11.11–11.104.
34. L. T. Sharpe, A. Stockman, W. Jagla, H. Jägle, A luminous efficiency function, $V^*(\lambda)$, for daylight adaptation. *J. Vis.* **5**, 948–968 (2005).
35. C. A. Curcio, K. A. Allen, K. R. Sloan, C. L. Lerea, J. B. Hurley, I. B. Klock, A. H. Milam, Distribution and morphology of human cone photoreceptors stained with anti-blue opsin. *J. Comp. Neurol.* **312**, 610–624 (1991).
36. K. Bumsted, A. Hendrickson, Distribution and development of short-wavelength cones differ between *Macaca* monkey and human fovea. *J. Comp. Neurol.* **403**, 502–516 (1999).
37. C. J. Ng, R. Blake, M. S. Banks, D. Tadin, G. Yoon, Optics and neural adaptation jointly limit human stereovision. *Proc. Natl. Acad. Sci. U.S.A.* **118**, e2100126118 (2021).
38. A. B. Watson, A. J. Ahumada, Predicting visual acuity from wavefront aberrations. *J. Vis.* **8**, 17.1–17.1719 (2008).
39. L. Zheleznyak, M. J. Kim, S. MacRae, G. Yoon, Impact of corneal aberrations on through-focus image quality of presbyopia-correcting intraocular lenses using an adaptive optics bench system. *J Cataract Refract Surg* **38**, 1724–1733 (2012).
40. L. N. Thibos, X. Hong, A. Bradley, R. A. Applegate, Accuracy and precision of objective refraction from wavefront aberrations. *J. Vis.* **4**, 329–351 (2004).
41. W. S. Geisler, Physical limits of acuity and hyperacuity. *J. Opt. Soc. Am. A* **1**, 775–782 (1984).
42. W. S. Geisler, Sequential ideal-observer analysis of visual discriminations. *Psychol. Rev.* **96**, 267–314 (1989).
43. C. Benedi-Garcia, M. Vinas, C. Dorronsoro, S. A. Burns, E. Peli, S. Marcos, Vision is protected against blue defocus. *Sci. Rep.* **11**, 352 (2021).
44. J. C. Hay, H. L. Pick, E. Rosser, Adaptation to chromatic aberration by the human visual system. *Science* **141**, 167–169 (1963).
45. L. N. Thibos, A. Bradley, X. Zhang, Effect of ocular chromatic aberration on monocular visual performance. *Optom. Vis. Sci.* **68**, 599–607 (1991).
46. M. A. Webster, M. A. Georgeson, S. M. Webster, Neural adjustments to image blur. *Nat. Neurosci.* **5**, 839–840 (2002).
47. R. J. Sharman, P. V. McGraw, J. W. Peirce, Luminance cues constrain chromatic blur discrimination in natural scene stimuli. *J. Vis.* **13**, 14 (2013).
48. F. A. A. Kingdom, J. Bell, C. Haddad, A. Bartsch, Perceptual scales for chromatic and luminance blur in noise textures. *J. Vis.* **15**, 6 (2015).
49. B. A. Wandell, *Foundations of Vision* (Sinauer Associates, 1995).
50. P. B. Kruger, S. Mathews, K. R. Aggarwala, N. Sanchez, Chromatic aberration and ocular focus: Fincham revisited. *Vision Res.* **33**, 1397–1411 (1993).
51. P. B. Kruger, K. R. Aggarwala, S. Bean, S. Mathews, Accommodation to stationary and moving targets. *Optom. Vis. Sci.* **74**, 505–510 (1997).
52. D. I. Flitcroft, A neural and computational model for the chromatic control of accommodation. *Vis. Neurosci.* **5**, 547–555 (1990).
53. F. J. Rucker, P. B. Kruger, The role of short-wavelength sensitive cones and chromatic aberration in the response to stationary and step accommodation stimuli. *Vision Res.* **44**, 197–208 (2004).
54. S. Mathews, P. B. Kruger, Spatiotemporal transfer function of human accommodation. *Vision Res.* **34**, 1965–1980 (1994).
55. D. A. Owens, A comparison of accommodative responsiveness and contrast sensitivity for sinusoidal gratings. *Vision Res.* **20**, 159–167 (1980).
56. D. H. Kelly, Spatio-temporal frequency characteristics of color-vision mechanisms. *J. Opt. Soc. Am.* **64**, 983 (1974).
57. D. J. McKeefry, I. J. Murray, J. J. Kulikowski, Red–green and blue–yellow mechanisms are matched in sensitivity for temporal and spatial modulation. *Vision Res.* **41**, 245–255 (2001).
58. T. Wachtler, T.-W. Lee, T. J. Sejnowski, Chromatic structure of natural scenes. *J. Opt. Soc. Am. A* **18**, 65 (2001).
59. Y. Gu, G. E. Legge, Accommodation to stimuli in peripheral vision. *J. Opt. Soc. Am. A* **4**, 1681–1687 (1987).
60. A. Hartwig, W. N. Charman, H. Radhakrishnan, Accommodative response to peripheral stimuli in myopes and emmetropes. *Ophthalmic Physiol. Opt.* **31**, 91–99 (2011).
61. V. Labhishetty, S. A. Cholewiak, M. S. Banks, Contributions of foveal and non-foveal retina to the human eye's focusing response. *J. Vis.* **19**, 18 (2019).
62. T. J. Gawne, R. Grytz, T. T. Norton, How chromatic cues can guide human eye growth to achieve good focus. *J. Vis.* **21**, 11 (2021).
63. P.-C. Huang, Y.-C. Hsiao, C.-Y. Tsai, D.-C. Tsai, C.-W. Chen, C.-C. Hsu, S.-C. Huang, M.-H. Lin, Y.-M. Liou, Protective behaviours of near work and time outdoors in myopia prevalence and progression in myopic children: A 2-year prospective population study. *Br. J. Ophthalmol.* **104**, 956–961 (2020).
64. P.-W. Ku, A. Steptoe, Y.-J. Lai, H.-Y. Hu, D. Chu, Y.-F. Yen, Y. Liao, L.-J. Chen, The associations between near visual activity and incident myopia in children. *Ophthalmology* **126**, 214–220 (2019).
65. C. Lanca, J. C. Yam, W. Jiang, Y. Tham, M. Hassan Emamian, C. Tan, Y. Guo, H. Liu, H. Zhong, D. Zhu, Y. Hu, R. Saxena, H. Hashemi, L. Chen, T. Wong, C. Cheng, C. Pang, H. Zhu, C. Pan, Y. B. Liang, A. Fotouhi, H. Bi, J. B. Jonas, S. Saw, The Asian Eye Epidemiology Consortium (AEEC), Near work, screen time, outdoor time and myopia in schoolchildren in the Sunflower Myopia AEEC Consortium. *Acta Ophthalmol.* **100**, 302–311 (2022).
66. Z. Lin, B. Vasudevan, G. Y. Mao, K. J. Ciuffreda, V. Jhanji, X. X. Li, H. J. Zhou, N. L. Wang, Y. B. Liang, The influence of near work on myopic refractive change in urban students in Beijing: A three-year follow-up report. *Graefes Arch. Clin. Exp. Ophthalmol.* **254**, 2247–2255 (2016).
67. O. Pärssinen, M. Kauppinen, Associations of near work time, watching TV, outdoors time, and parents' myopia with myopia among school children based on 38-year-old historical data. *Acta Ophthalmol.* **100**, e430–e438 (2022).
68. F. J. Rucker, J. Wallman, Chick eyes compensate for chromatic simulations of hyperopic and myopic defocus: Evidence that the eye uses longitudinal chromatic aberration to guide eye-growth. *Vision Res.* **49**, 1775–1783 (2009).
69. P.-C. Wu, C.-T. Chen, L.-C. Chang, Y.-Z. Niu, M.-L. Chen, L.-L. Liao, K. Rose, I. G. Morgan, Increased time outdoors is followed by reversal of the long-term trend to reduced visual acuity in Taiwan primary school students. *Ophthalmology* **127**, 1462–1469 (2020).
70. A. Roorda, S. A. Cholewiak, S. Bhargava, N. H. Ivzan, F. LaRocca, D. Nankivil, M. S. Banks, The visual benefits of correcting longitudinal and transverse chromatic aberration. *J. Vis.* **23**, 3 (2023).
71. K. R. Aggarwala, E. S. Kruger, S. Mathews, P. B. Kruger, Spectral bandwidth and ocular accommodation. *J. Opt. Soc. Am. A* **12**, 450 (1995).
72. M. Fernandez-Alonso, A. P. Finch, G. D. Love, J. C. A. Read, Ocular accommodation and wavelength: The effect of longitudinal chromatic aberration on the stimulus–response curve. *J. Vis.* **24**, 11 (2024).
73. C. A. Johnson, Effects of luminance and stimulus distance on accommodation and visual resolution. *J. Opt. Soc. Am.* **66**, 138–142 (1976).
74. L. N. Thibos, R. A. Applegate, J. T. Schwiegerling, R. Webb, Standards for reporting the optical aberrations of eyes. *J. Refract. Surg.* **18**, S652–S660 (2002).
75. L. N. Thibos, M. Ye, X. Zhang, A. Bradley, The chromatic eye: A new reduced-eye model of ocular chromatic aberration in humans. *Appl. Optics* **31**, 3594–3600 (1992).
76. D. Nankivil, N. P. Cottaris, D. H. Brainard, Theoretical impact of chromatic aberration correction on visual acuity. *Biomed. Opt. Express* **15**, 3265 (2024).
77. R. E. Bedford, G. Wyszecki, Axial chromatic aberration of the human eye. *J. Opt. Soc. Am.* **47**, 564–565 (1957).
78. D. P. Cooper, P. L. Pease, Longitudinal chromatic aberration of the human eye and wavelength in focus. *Am. J. Optom. Physiol. Opt.* **65**, 99–107 (1988).
79. P. A. Howarth, A. Bradley, The longitudinal chromatic aberration of the human eye, and its correction. *Vision Res.* **26**, 361–366 (1986).
80. G. Wald, D. R. Griffin, The change in refractive power of the human eye in dim and bright light. *J. Opt. Soc. Am.* **37**, 321–336 (1947).

81. C. Ware, Human axial chromatic aberration found not to decline with age. *Graefes Arch. Clin. Exp. Ophthalmol.* **218**, 39–41 (1982).
82. D. Nankivil, T. D. Raymond, G. J. Hofmann, D. R. Neal, "Estimating visual acuity from a single wavefront measurement" in *Ophthalmic Technologies XXX*, F. Manns, P. G. Söderberg, A. Ho, Eds. (SPIE, 2020), p. 73.
83. L. Llorente, L. Diaz-Santana, D. Lara-Saucedo, A. S. Marcos, Aberrations of the human eye in visible and near infrared illumination. *Optom. Vis. Sci.* **80**, 26–35 (2003).
84. D. A. Atchison, M. J. Collins, C. F. Wildsoet, J. Christensen, M. D. Waterworth, Measurement of monochromatic ocular aberrations of human eyes as a function of accommodation by the howland aberroscope technique. *Vision Res.* **35**, 313–323 (1995).
85. H. Cheng, J. K. Barnett, A. S. Vilupuru, J. D. Marsack, S. Kasthurirangan, R. A. Applegate, A. Roorda, A population study on changes in wave aberrations with accommodation. *J. Vis.* **4**, 272–280 (2004).
86. J. C. He, S. A. Burns, S. Marcos, Monochromatic aberrations in the accommodated human eye. *Vision Res.* **40**, 41–48 (2000).
87. C. R. Cavonius, O. Estévez, Contrast sensitivity of individual colour mechanisms of human vision. *J. Physiol.* **248**, 649–662 (1975).
88. M. J. Sankeralli, K. T. Mullen, Estimation of the L-, M-, and S-cone weights of the postreceptoral detection mechanisms. *J. Opt. Soc. Am. A* **13**, 906 (1996).
89. C. Nakatsuka, Accommodative lag under habitual seeing conditions: Comparison between adult myopes and emmetropes. *Jpn. J. Ophthalmol.* **47**, 291–298 (2003).

Acknowledgments: We thank S. Singh, G. Meng, and E. Harb for helpful feedback on the manuscript. **Funding:** This work was supported by National Science Foundation Award no. 2041726 to E.A.C., National Institutes of Health Award K99EY036497 to B.M.C., and the Center for Innovation in Vision and Optics. **Author contributions:** Conceptualization: B.M.C., M.S.B., D.N., A.R., and E.A.C. Methodology: B.M.C., M.S.B., D.N., A.R., and E.A.C. Software: B.M.C. Validation: B.M.C. Formal analysis: B.M.C. Investigation: B.M.C. Resources: A.R. Data curation: B.M.C. Visualization: B.M.C., D.N., and E.A.C. Supervision: M.S.B., D.N., A.R., and E.A.C. Project administration: B.M.C. and E.A.C. Funding acquisition: B.M.C. and E.A.C. Writing—original draft: B.M.C. and E.A.C. Writing—review and editing: B.M.C., M.S.B., D.N., A.R., and E.A.C. **Competing interests:** At the time this work was conducted, D.N. had employment, patent, and personal financial interest in Johnson & Johnson Vision. Presently, D.N. has employment and personal financial interest in Alcon Laboratories. The authors declare that they have no other competing interests. **Data, code, and materials availability:** All data and code needed to evaluate and reproduce the results in the paper are publicly available on Zenodo (https://zenodo.org/records/18180188) and OSF (https://osf.io/k9bdh/overview). This study did not generate new materials.

Submitted 15 July 2025
Accepted 18 February 2026
Published 1 April 2026
10.1126/sciadv.aea5693

ScienceAdvances

Focusing on color: How the eye chooses which wavelength to see best

Benjamin M. Chin, Martin S. Banks, Derek Nankivil, Austin Roorda, and Emily A. Cooper

Sci. Adv. **12** (14), eaea5693. DOI: 10.1126/sciadv.aea5693

Science Advances (ISSN 2375-2548) is published by the American Association for the Advancement of Science. 1200 New York Avenue NW, Washington, DC 20005. The title *Science Advances* is a registered trademark of AAAS.